Nonlinear Ultrasonic Stimulated Thermography for Damage Assessment in Isotropic Fatigued Structures

Gian Piero Malfense Fierro, Danielle Calla, Dmitri Ginzburg, Francesco Ciampa and Michele Meo

University of Bath, Materials Research, Department of Mechanical Engineering, Claverton Down, Bath, UK

Abstract

Traditional non-destructive evaluation (NDE) and structural health monitoring (SHM) systems are used to analyse that a structure is free of any harmful damage. However, these techniques still lack sensitivity to detect the presence of material micro-flaws in the form of fatigue damage and often require time-consuming procedures and expensive equipment. This research work presents a novel "nonlinear ultrasonic stimulated thermography" (NUST) method able to overcome some of the limitations of traditional linear ultrasonic/thermography NDE-SHM systems and to provide a reliable, rapid and cost effective estimation of fatigue damage in isotropic materials. Such a hybrid imaging approach combines the high sensitivity of nonlinear acoustic/ultrasonic techniques to detect micro-damage, with local defect frequency selection and infrared imaging. When exciting structures with an optimised frequency, nonlinear elastic waves are observed and higher frictional work at the fatigue damaged area is generated due to clapping and rubbing of the crack faces. This results in heat at cracked location that can be measured using an infrared camera. A Laser Vibrometer (LV) was used to evaluate the extent that individual frequency components contribute to the heating of the damage region by quantifying the out-of-plane velocity associated with the fundamental and second order harmonic responses. It was experimentally demonstrated the relationship between a nonlinear ultrasound parameter (β_{ratio}) of the material nonlinear response to the actual temperature rises near the crack. These results demonstrated that heat generation at damaged regions could be amplified by exciting at frequencies that provide nonlinear responses, thus improving the imaging of material damage and the reliability of NUST in a quick and reproducible manner.

Keywords: Thermosonics, Thermography, Nonlinear Ultrasound, Laser Vibrometer

1.1. Introduction

The reliability of traditional non-destructive evaluation (NDE) and structural health monitoring (SHM) methodologies depends to a great extent on the sensitivity of the technique and the capabilities and experience of the inspectors or technicians. For decades, ultrasonic methods have been an excellent tool for structural monitoring and still are. Conventional linear ultrasonic (LU) techniques such as C-scan and linear array scanning are quite advanced and mature, and are frequently used in industry to monitor metallic and composite components [1], [2]. However, LU techniques are not able to detect small defects before they grow to a critical size of few millimetres as the material damage signature can be masked by other information contained in the measured signal, such as reflections from boundaries, diffraction from edges, dispersion and mode conversion. In addition, LU methods such as C-Scan are point testing so that they are intrinsically slow in inspecting large areas, and require a reliable coupling agent (usually water). Hence, these techniques are ineffective in detecting contact-type damage such as corrosion and micro-cracking in metals. Infrared (IR) thermography is a valid alternative to LU methods for rapid material inspection, and it has been estimated to be up to thirty times quicker than underwater ultrasonic C-scan techniques, illustrating the ability to rapidly inspect large areas of composite materials [3]. However, major problems arise when the defect is too deep to be reached by a significant amount of heat or when the damage interfaces are in contact (as in the case of micro-cracks), hence allowing heat transmission and no detection of material flaws. Thermosonics (also known as “ultrasonically stimulated thermography” or “vibro-thermography”) is an alternative means of thermography that is currently gaining considerable interest worldwide for its many potential applications [4]. Thermosonic

inspection involves the generation of powerful vibrations in a test piece to cause frictional heating at crack surfaces that can be imaged by an IR camera. Indeed, under sonic or ultrasonic mechanical vibrations, a delamination may behave like an internal heat source due to friction between the rubbing faces and viscoelastic hysteresis heating at the defect area [5]. Typically these vibrations are produced by an ultrasonic plastic welding horn being pressed against a surface on the part under inspection. The level of acoustic power is of the order of kW, with an operating frequency ranging between 15 and 40 kHz. However, the ultrasonic horn used in thermosonics is a bulky and a crude means of exciting high-power vibrations. The coupling between the test specimen and the horn typically results in an uncontrolled generation of frequency components known as "acoustic chaos". Such a condition makes this method highly non-reproducible, thus leading to cracks being undetected if sufficient vibrational energy is not applied at the crack location [6]. This inevitably limits the use of thermosonics for industrial applications. There is therefore a need to develop NDE-SHM techniques that will detect and visualise both surface and internal micro-defects quickly and reliably.

Nonlinear elastic wave spectroscopy (NEWS) techniques are an innovative class of ultrasonic NDE and SHM inspection methods that measure nonlinear elastic effects in the kHz frequency range to reveal the presence of surface and sub-surface micro-flaws [7], [8]. Indeed, the interactions of ultrasonic waves with early stage material damage and micro-cracks generates either the frictional heating (rubbing) or the transfer of deformation energy (clapping). This results in three different failure modes: tensile mode (clapping), in-plane shear mode (rubbing), and anti-plane shear mode (rubbing). The acoustic power within a given material is dependent on material resonance, with material resonance determining the velocity of the different crack interfaces, which can be related to frictional heating. As a result of these interactions, nonlinear material effects such as harmonics and sub-harmonics of the single driving frequency, as well as modulation (or sidebands) of two input frequencies can be generated [9]. Compared to LU methods, these techniques have shown an extreme sensitivity in diagnosing material micro-defects such as porosity, inlcusions and early stage damage in the form of micro-cracks, delaminations, clapping areas and adhesive bond weakening [10], [11] and [12]. Nevertheless, from a theoretical point of view, it is well-known that the classical theory of nonlinear acoustic/ultrasonic phenomena (i.e. the "anharmonic elastic theory" from Landau [13]) does not describe the full set of nonlinear material effects observed in experiments dealing with material micro-damage. A recent study showed that if the excitation frequency matches the local resonance frequency of material damage, the vibration amplitude of nonlinear elastic phenomena can be increased [14]. Such effects, such as local defect resonance (LDR) [15], is a new avenue for material science and physics of nonlinear acoustic/ultrasonic phenomena that will be theoretically and experimentally analysed in this paper to decrease the input power of the ultrasonic excitation signals ([16] and [17]).

In this research work, NEWS methods were combined with thermography and standard PZT transducers in order to develop a novel hybrid NDE-SHM inspection system, namely "nonlinear ultrasonic stimulated thermography (NUST)", which is capable of providing a quick and reliable detection and localisation of micro-flaws. Whilst NEWS methods provided a first screening of damage by measuring the material nonlinear response, the resulting thermal heat originated at the crack location was measured with a standard thermographic method. A fatigued aluminium coupon was used to evaluate crack (frictional) heating by selecting the defect resonance excitation frequencies that resulted in the maximum generation of heat at the crack interfaces. This was accomplished by performing a modal analysis of the fatigued sample both experimentally (with a laser vibrometer, LV) and numerically (using the finite element method) in order to identify high velocity regions near the crack associated with the second harmonic material nonlinear response. As a result, a novel nonlinear ultrasound parameter (β_{ratio}) was created to assess how the variations of out-of-plane velocity between the fundamental frequency and second harmonic response affect the heat generation and the total frictional work. This allowed increasing the reliability of NUST.

1.2. Theoretical and Experimental Frictional Work

By determining the frictional work attributed to the fundamental and second harmonics it is possible to characterise the main heating components, and thus evaluate benefits of exciting at defect resonance. The frictional work (W_f) performed at defect faces leads to heating of defects like cracks, and can be described by the equation below [5]:

$$W_f = \mu F_N s = \mu F_N \int_0^T \left| V'_{TOT}(t) \right| \mathrm{d}t \tag{1}$$

where: μ is the coefficient of friction, F_N the normal force that presses the defect faces together, s is the total way the crack faces moved against each other and the primed velocity $V'_{TOT}(t)$ is the relative velocity of the crack faces, which can be defined as:

$$\begin{aligned} V'_{TOT}(t) &\cong \sum_{n=1}^{2} v_n \sin(n2\pi f_1 t) + \sum_{m=3}^{\infty} v_m \sin(m2\pi f_1 t) \\ &= v_1 \sin(2\pi f_1 t) + v_2 \sin(4\pi f_1 t) + o\left[\sum_{m=3}^{\infty} v_m \sin(m2\pi f_1 t) \right], \\ &= V'_{f1}(t) + V'_{2f1}(t) + o\left[V'_{mf1}(t)\right] \end{aligned} \tag{2}$$

where: v_1 and v_2 are the amplitudes of the defect resonance frequency (f_1) and the second order nonlinear contribution ($2f_1$), respectively. According to Eq. (2), the total contribution of the relative velocity of crack faces is mainly given by a superposition of the fundamental and second harmonic frequency component generated at the LDR, whilst the higher order nonlinear contributions are considered negligible. Substituting Eq. (2) into Eq. (1) yields:

$$\begin{aligned} W_f &= \mu F_N \int_0^T \left[\left| V'_{f1}(t) + V'_{2f1}(t) \right| \right] \mathrm{d}t = \mu F_N \left[\int_0^T \left| V'_{f1}(t) \right| dt + \int_0^T \left| V'_{2f1}(t) \right| \mathrm{d}t \right] \\ &= \mu F_N \left(s_{f1} + s_{2f1} \right) \end{aligned} \tag{3}$$

However, due to the difficulty in experimentally determining the normal force (F_N) over the cracked region, the assumption that frictional work (and heating) is proportional to the relative displacement $\left(s_{f1} + s_{2f1}\right)$ of the crack faces has been made. This will be referred to as "frictional work contribution" W_{fc}, and is defined as:

$$W_f \propto W_{fc} = s_{f1} + s_{2f1} \tag{4}$$

Since μ is a constant of the material used [18] and the dominating factor in the frictional work W_f is the variation of relative displacement $\left(s_{f1} + s_{2f1}\right)$, the assumption $W_f \propto W_{fc}$ in Eq. (4) is valid. In addition, a linear relationship between crack heating and excitation time has been found in this research (as will be shown later in this paper), thus Eq. (4) can be used to adequately explain the frictional work.

As mentioned earlier, further harmonics, at twice and three times the fundamental frequency, have been shown to be generated by damage/defects [19], [20]. The production of these harmonics and sub-harmonics are generally agreed to be beneficial for crack heating [21]. The fundamental equation used to determine the second-order nonlinearity of the LDR frequency provides essential information that

allow nonlinearity (due to damage) to be quantified and analysed. This can be described by the equation below [21]:

$$\beta = \frac{8A_2}{A_1^2 k^2 a_1} \approx \frac{A_2}{A_1^2} \tag{5}$$

where: A_1 and A_2 are the respective frequency amplitudes of the fundamental (defect resonance) and second harmonics (f_1 and $2f_1$) of the recorded time domain waveform, k is the wavenumber, and a_1 is the propagation distance. For practical reason, β is usually calculated as the ratio of the second harmonic amplitude over the fundamental squared, this has been used in for the purposes of this work. Furthermore, in order to assess the effect of nonlinearity around the cracked region, a parameter here named as β_{ratio}, was obtained as follows:

$$\beta_{ratio} = \frac{\beta_{damaged}}{\beta_{undamaged}} = \frac{A_2 / A_1^2 \big|_{damaged}}{A_2 / A_1^2 \big|_{undamaged}} \tag{6}$$

where $\beta_{damaged}$ is the second order nonlinear parameter calculated at the damaged region (i.e. at the crack location), whilst $\beta_{undamaged}$ is β measured in the undamaged area of the fatigued sample near the crack. In this manner, it was possible to evaluate that frequency that gave rise to the largest nonlinearity near the cracked area.

1.3. Equipment and Experimental Setup

The experiment uses a series of highly sensitive equipment in order to assess and measure various key aspects of a fatigue crack, such as temperature and out-of-plane velocity. The metal coupon was an aluminium plate (AA2024) specifically designed according to ASTM standards for fatigue crack growth (Figure 1). The fatigue coupon had a length of 185mm, width of 50 mm and thickness of 8 mm. A 2.4 mm notch was machined and then tapered in from both edges to a fine point, with a total depth of 8 mm. The fatigue crack was induced through a fatigue machine (Instron 8801), which allowed the plate to be fixed with hydraulic clamps and apply low-cycle fatigue loading until a significant fatigue crack had propagated. An analysis of the crack was performed with an optic microscope (Leyca M205 C). LV testing and thermography testing relied on the excitation of the coupon from the transducer location highlighted in Figure 1. The transducer was located 30mm to the left of the centre of the notch and 20 mm down.

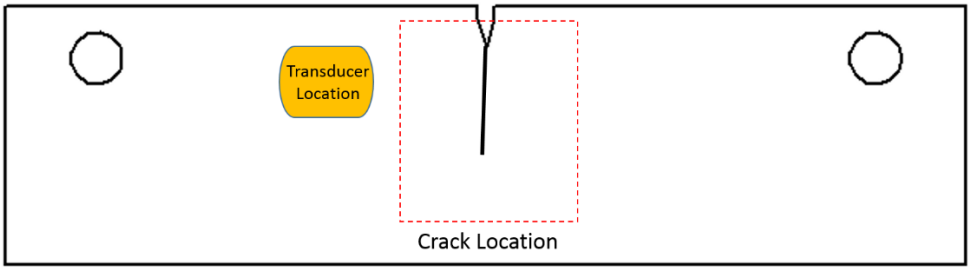

Figure 1: Fatigue Coupon Layout.

Continuous excitation was used to stimulate the fatigue coupon using multiple frequencies at 80 Vpp. The responses of these excitations were then measured at a sampling frequency of 1 MHz. The input signals were generated using a function generator (TTI 50 MHz Pulse Generator T6501) linked to an amplifier (Falco Systems DC 5 MHz High Voltage WMA-300), and applied to the structure with a piezoelectric active transducer (McWade Acoustic Emission Sensor Type NS3303 with width of 2 cm, length of 2.3 cm and thickness of 1 cm) with a resonance frequency of 150 kHz. The direct out-of-plane

vibration responses were captured using a highly sensitive LV (Polytec PSV-A-420) with a grid of 1815 points (55x33). The grid covered the area around the fatigue crack (Figure 2 (a)). The fatigue crack grew to a length of 10.13 mm and then split into two further cracks of 2.94 mm and 2.2 mm as outlined in Figure 2 (b). A thermal camera (Janos Technology 40486, with Asio lenses of 13 mm) was used to capture heating at each frequency investigated. Environmental conditions were carefully controlled using thermocouples along the structure. Thus an accurate relative temperature gradient could be recorded at the start of ultrasonic excitation, which was conducted for a total time of 36 seconds with the thermal camera capturing at a sampling rate of 15 frames per second. An emissive coating was used to coat the samples, and background subtraction used to evaluate crack heating.

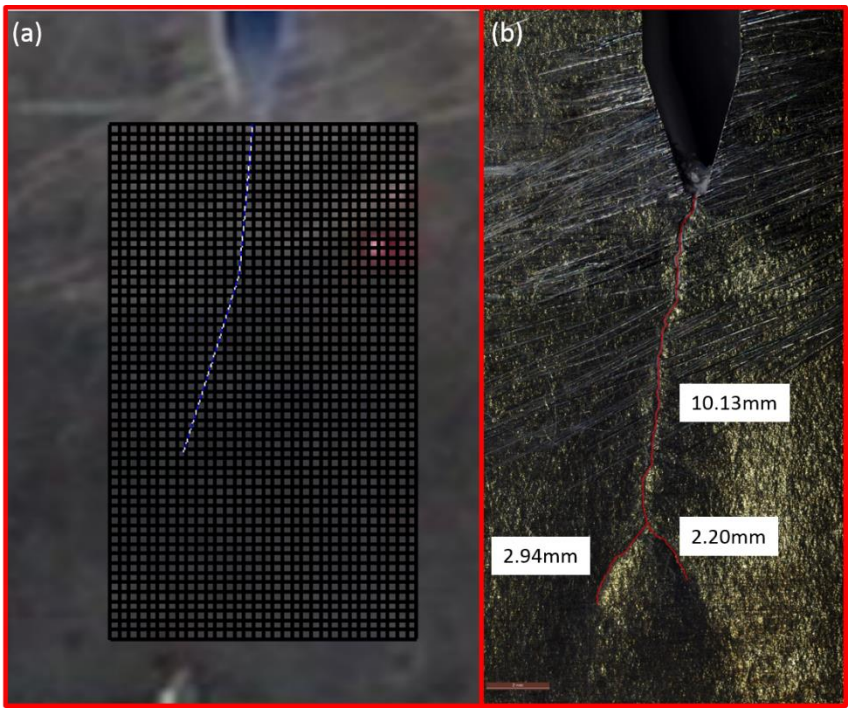

Figure 2: Laser vibrometer scan region and points (55 x 33, 1815 points) (a), fatigue crack microscope inspection with crack lengths (b).

1.4. Modal Analysis and Resonant Frequency Evaluation

Modal analysis was performed using FEA software LS-DYNA® on the undamaged aluminium sample for the frequencies shown in Table 1 in order to define the mode shape associated to each frequency. In the numerical analysis, simple free boundary conditions were used.

Table 1: Frequencies selected for undamaged sample modal analysis.

Frequency (Hz)
110000, 112000, 115156, 115531, 116531, 117281, 118188, 118500, 118875,119406, 120000

The main aim was to determine the mode shape near the expected crack region in order to understand the potential for rubbing and/or clapping to occur. It is well documented that damage within a structure alters stiffness and thus changes the modal parameters. Further to this, the severity and location of damage will affect each vibration mode differently, having a strong effect on some modes and weak effects on others. The LV was used to determine the out-of-plane velocities (Figure 3) for various excitation frequencies.

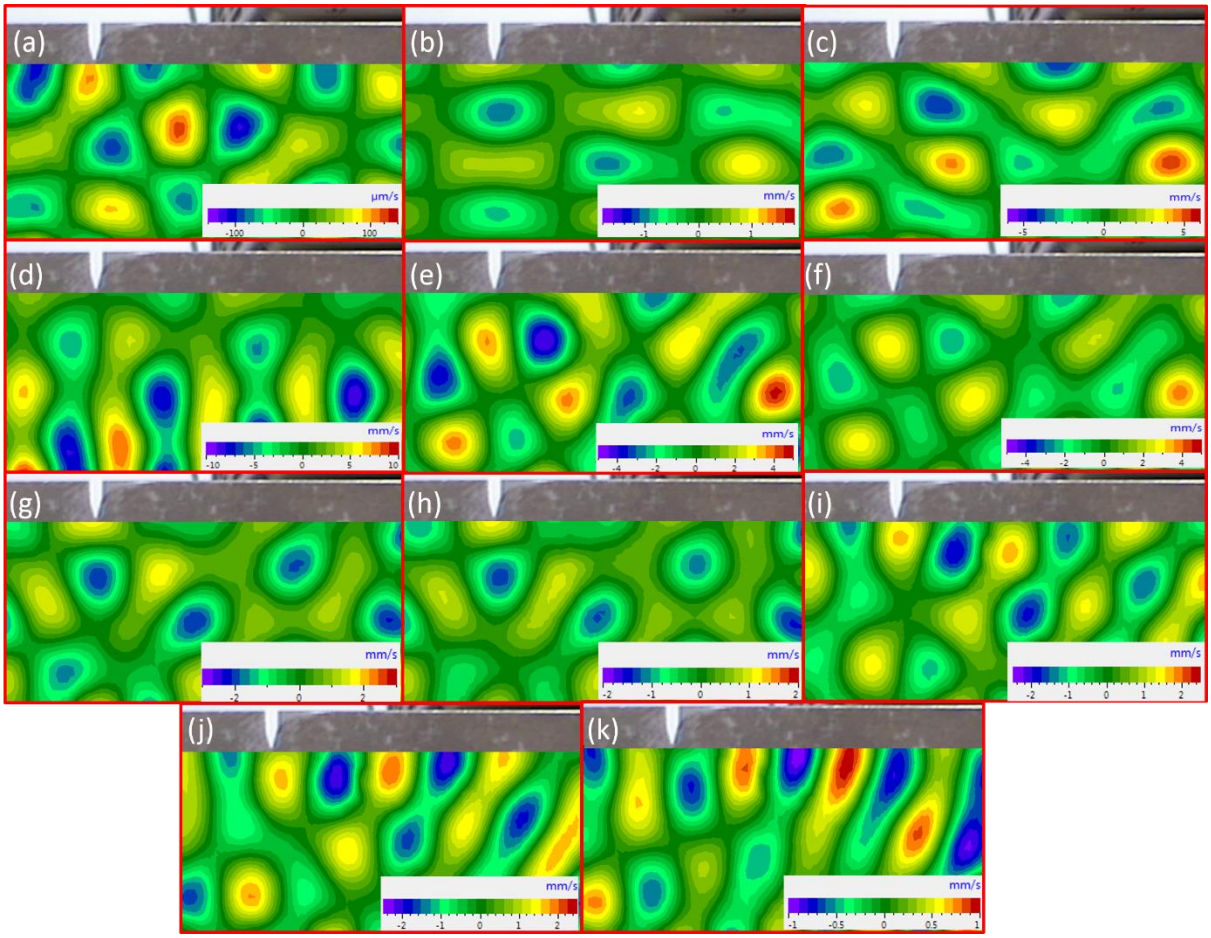

Figure 3: Mode shapes for 110000 Hz (a), 1120000 Hz (b), 115156 Hz (c), 115531 Hz (d), 116531 Hz (e), 117281 Hz (f), 118188 Hz (g), 118500 Hz (h), 118875 Hz (i), 119406 Hz (j) and 120000 Hz (k).

The defect resonance frequency evaluation of the linear and nonlinear response was conducted using a sweep signal. Figure 4 below outlines the average frequency response for the LV evaluated area (Figure 2), highlighting the fundamental (f_1) (between 110 kHz and 120 kHz) and second harmonic response ($2f_1$) (between 220 kHz and 240 kHz). Eleven frequencies were selected from the frequency response of the sample and the criteria for each selection is highlighted below.

Table 2: Frequency Selection Criteria Damaged Sample.

Frequency (Hz)	Reason:	Other Notes:
110000 (A)	Random Selection	
112000 (B)	Random Selection	
115078 (C)	High Second Harmonic Response	
115859 (D)	High Fundamental Response	High Second Harmonic Response
116406 (E)	High Second Harmonic Response	
117345 (F)	High Second Harmonic Response	
118320 (G)	High Second Harmonic Response	
118750 (H)	High Second Harmonic Response	High Fundamental Response
118820 (I)	High Fundamental Response	
119260 (J)	High Second Harmonic Response	
120000 (K)	Random Selection	

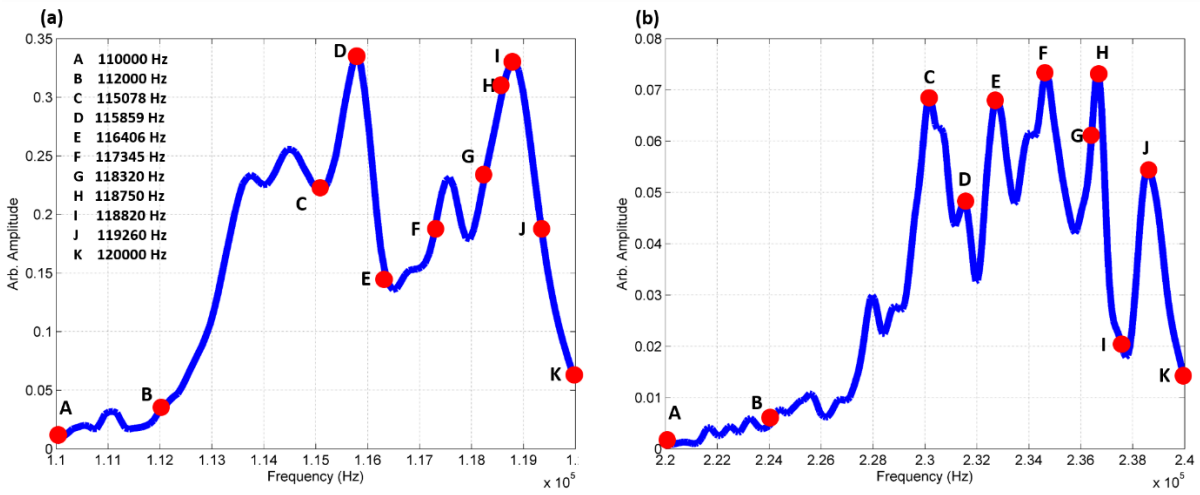

Figure 4: Comparison of average spectrum for the fundamental frequency response from 110 kHz to 120 kHz (a) and the second harmonic frequency response from 220 kHz to 240 kHz (b).

1.5. Laser Vibrometer Testing

A laser vibrometer was used to evaluate the out-of-plane amplitudes of f_1 and $2f_1$ for the fatigued coupon. The coupon was continuously excited using an ultrasound transducer at the frequencies chosen (Modal analysis was performed using FEA software LS-DYNA® on the undamaged aluminium sample for the frequencies shown in Table 1 in order to define the mode shape associated to each frequency. In the numerical analysis, simple free boundary conditions were used.

Table 1). The time domain signal was captured for the given grid area and a fast fourier transform (FFT) was completed to determine the maximum amplitudes. Figure 5 below shows f_1 and $2f_1$ for the evaluated region superimposed on the cracked region. It is clear to see that for this case f_1 occurs to the left of the crack (same side of excitation signal), whilst the second harmonic response occurs on the opposite side. This follows nonlinear ultrasound theory that further harmonic generation occurs at damage interfaces and dislocation positions, shown by: refelction of f_1 to the left of the crack interface, and propagation of further harmonic generation through the crack interface (clapping/rubbing) resulting in higher vibrational amplitude occuring on the opposite side.

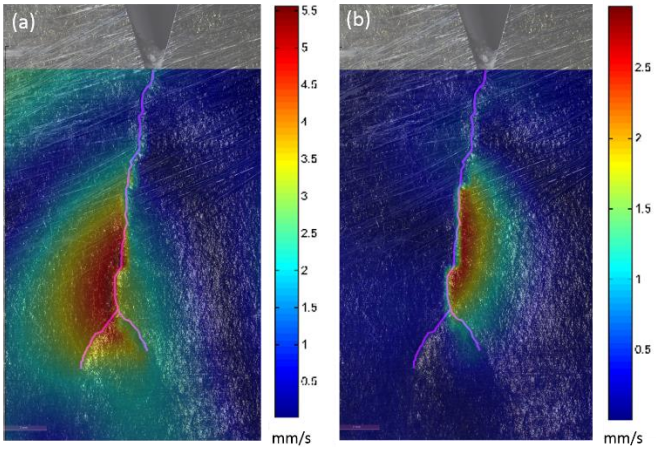

Figure 5: Fundamental Frequency f_1 (a) and second harmonic $2f_1$ (b) response superimposed over cracked region (115859 Hz).

It is expected that the combined interaction of the f_1 and $2f_1$ at opposite sides of the crack results in greater heating. Reliably evaluating which combination gives rise to the highest heating is the main aim of this investigation. Figure 6, Figure 7 and Figure 8 show the relative fundamental and second

harmonic responses for the frequencies tested. For the frequencies that exhibited large second harmonic responses there is a clear separation of f_1 and $2f_1$ on either side of the crack interface.

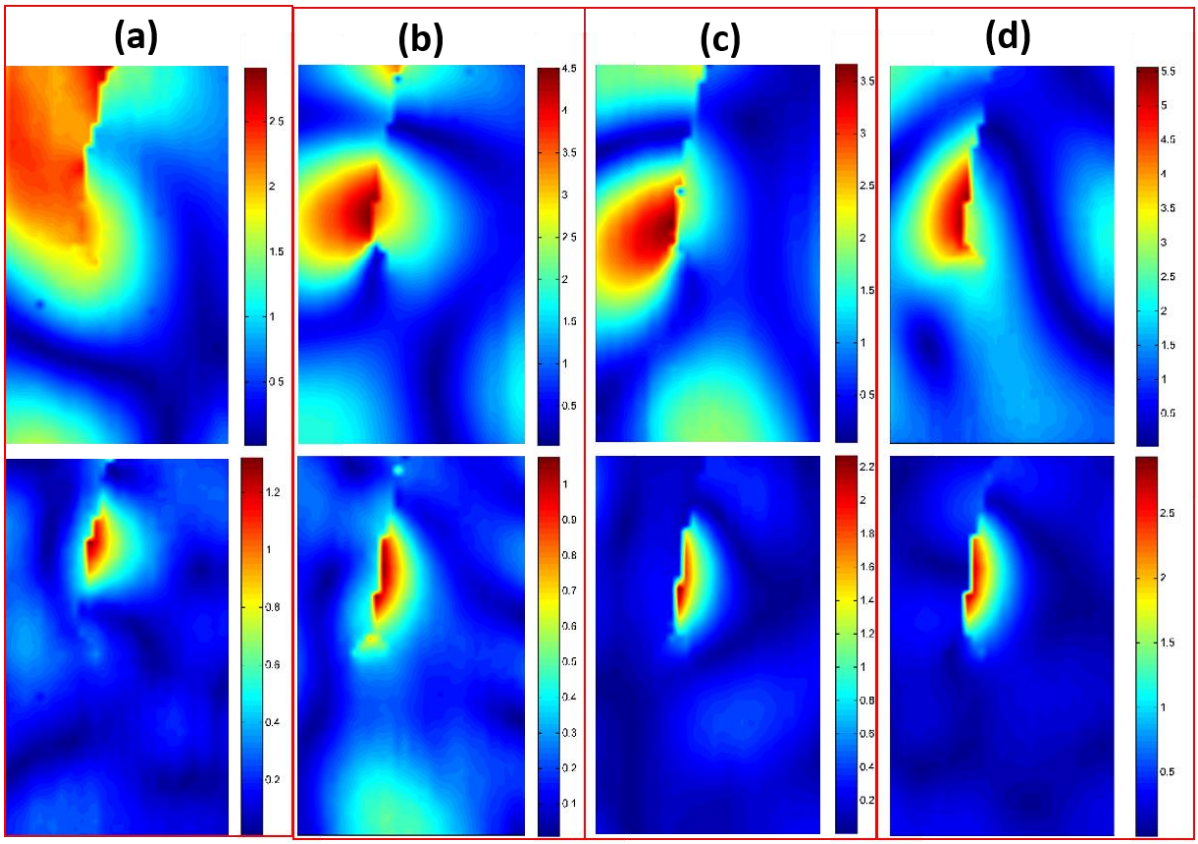

Figure 6: Fundamental (f_1 -top row) and second harmonic ($2f_1$ – bottom row) relative velocity contour plots (mm/s) for 110000 Hz (a), 112000 Hz (b), 115078 Hz (c) and 115859 Hz (d).

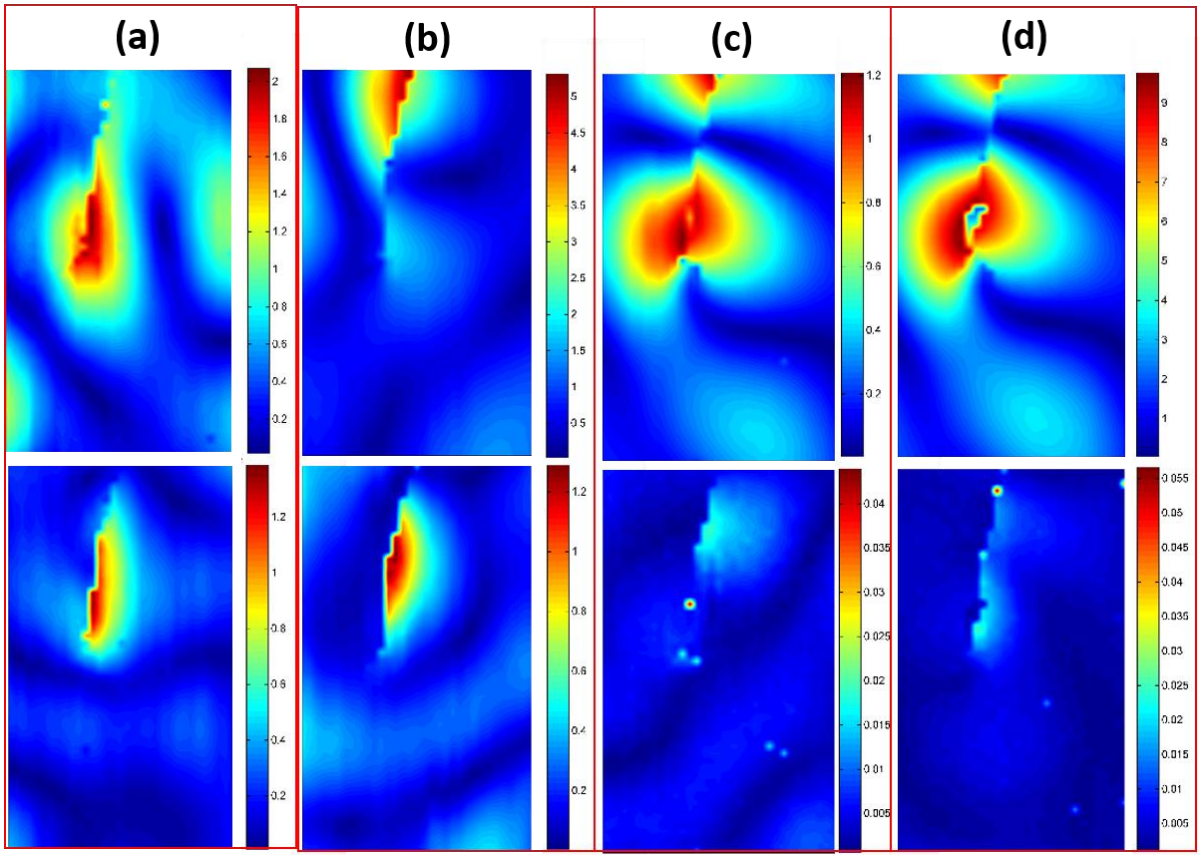

Figure 7: Fundamental (f_1 -top row) and second harmonic ($2f_1$ – bottom row) relative velocity contour plots (mm/s) for 116406 Hz (a), 117345 Hz (b), 118320 Hz (c) and 118750 Hz (d).

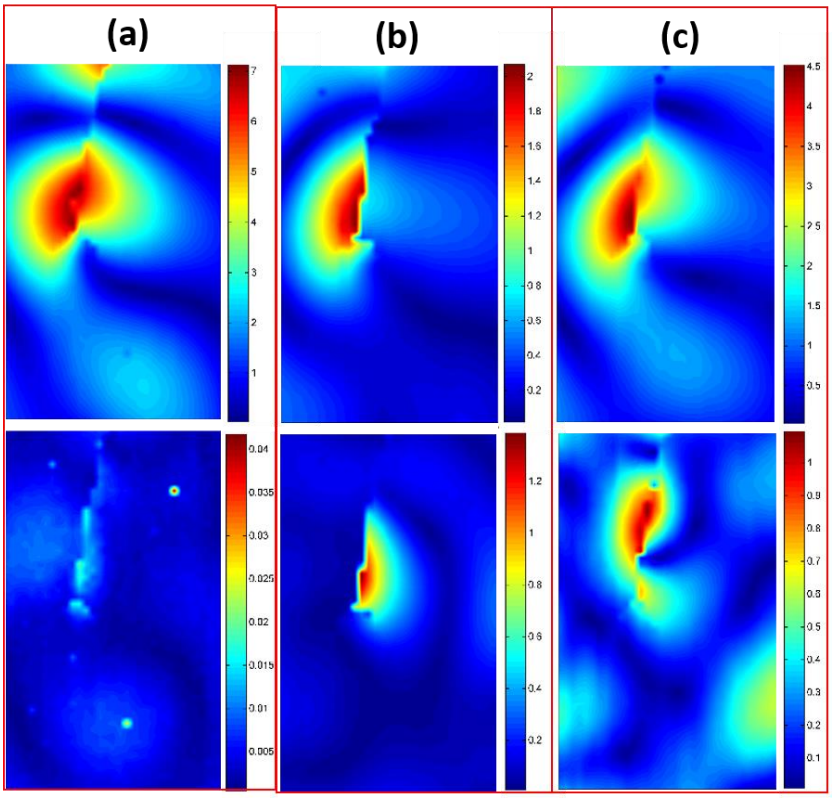

Figure 8: Fundamental (f_1 -top row) and second harmonic ($2f_1$ – bottom row) relative velocity contour plots (mm/s) for 118820 Hz (a), 119260 Hz (b) and 120000 Hz (c).

Figure 9 shows a comparison between the LV and the numerical finite element analysis (FEA) mode results for three frequencies. The FEA results show good qualitative agreement with those captured with the LV.

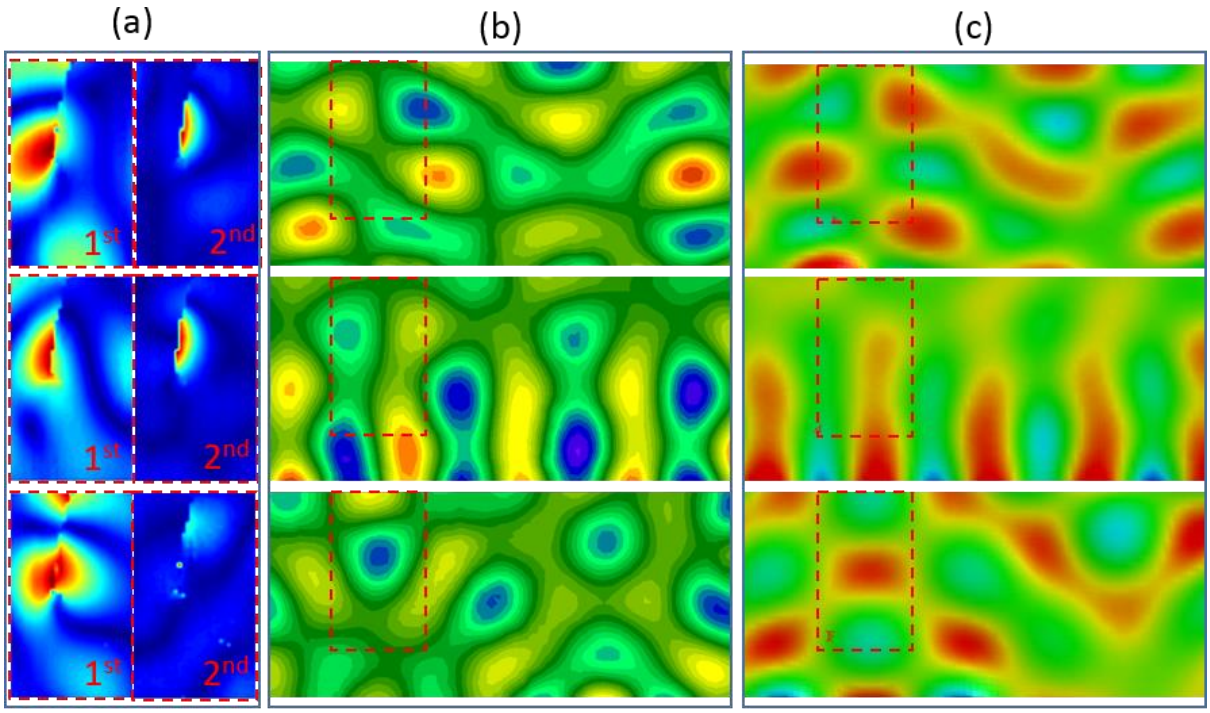

Figure 9: Damaged fundamental (f_1) and Second harmonic response ($2f_1$) (a) for 115078 Hz (top), 115859 Hz (middle) and 118320 Hz (bottom); undamaged mode shapes from LV (b) for 115156 Hz (top), 115531 Hz (middle) and 118500 Hz (bottom); and undamaged FEA mode results (c) with a frequency error of the simulation of -1.7% (top), -2.5% (middle) and -0.6% (bottom).

The modal shapes between the LV and the FEA results show good correlation in terms of response. By comparing the response of the fundamental and second harmonic of the damaged coupon to the undamaged modal shape it is clear that the position of out-of-plane min/max locations directly affects the amplitude and position of f_1 and $2f_1$ responses. In the event that the min/max locations occur over the cracked region (rather than on either side, frequencies 118320 Hz, 118500 Hz and 117850 Hz) there is a clear reduction in the production of the second harmonic. Whereas when min/max locations are either side of the cracked region there is a split between f_1 response (which is located on the same side of the excitation frequency) and the production of $2f_1$ which is located on the opposite side of the crack interface (with reference to the excitation signal). Furthermore the results suggest that when the fundamental and second harmonic responses are split either side of the crack, this results in greater out-of-plane rubbing of the crack interface, which should result in a greater generation of frictional heating.

The modal analysis was also carried out on the sample in the damaged state following the low-cyclic fatigue process. The fatigue crack was represented in the computational domain by careful modelling of the crack surface and assigning double nodes at the crack interface (total number of 3D solid elements was 1.107 million). Figure 10 shows one of the numerically determined natural modes using a FEA model of the specimen containing a fatigue crack.

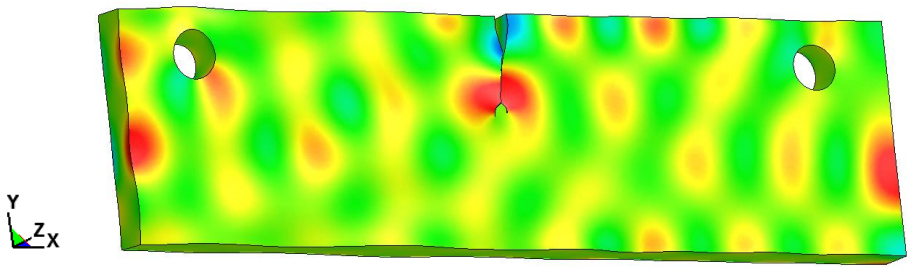

Figure 10: Mode shape determined via numerical modal analysis (LS-DYNA®), out-of-plane displacement at 117.28 kHz for the cracked structure.

Figure 11 illustrates a good correlation between the experimental (LV) and numerical results: only the modes that were characterised by the out-of-plane displacement of the order of magnitude larger than the in-plane were chosen from the results of modal analysis. As indicated in Figure 11, in the case of 118320 Hz, both sides of the crack displayed high out-of-plane velocity acting in-phase with each other. On the other hand, at 115859 Hz the crack sides were moving in opposite out-of-plane directions.

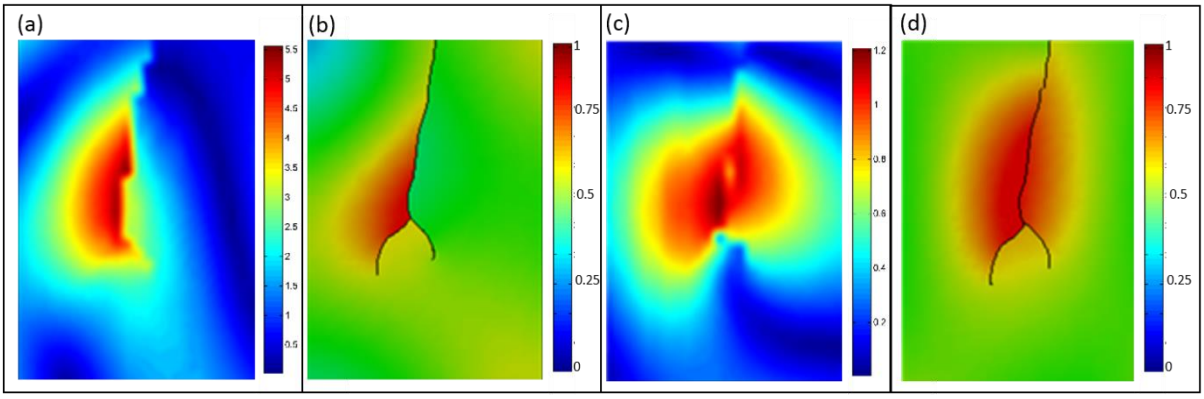

Figure 11: Comparison between the contours of the out-of-plane velocity (mm/s) obtained by means of LV experiments ((a) – 115.859 kHz, (c) – 118.320 kHz) and contours of the normalised out-of-plane displacement obtained via FEA modal analysis of the cracked structure ((b) – frequency error -2.6%, (d) – frequency error -2.6%,).

1.6. Nonlinear ultrasonic stimulated thermography testing

In order to determine the actual heating at the cracked interface, NUST testing was conducted using the experimental set-up outlined in section 1.2. Various relative temperature profiles were evaluated by capturing temperature changes (using an IR camera, Figure 13, Figure 14 and Figure 15) over time during ultrasound excitation at various points on the damaged coupon. Figure 12 shows the locations of the measured temperatures. By comparing the thermal gradients between the different excitation frequencies, it can be seen that the gradients are greater around the cracked region (red - Figure 12) relative to the surface position (undamaged, blue - Figure 12) and the crack tip (yellow - Figure 12). It should be noted that the excitation frequency was always conducted at the fundamental but the response of the second harmonic and heating differs. This is in agreement with the fundamental and second harmonic responses (outlined in Figure 6, Figure 7 and Figure 8) which show that the greatest relative displacement either occurs at the beginning (near the notch) or near the middle of the crack, and therefore heating in these areas should be greater. Figure 14 shows that when exciting at the fundamental frequency that gives rise to the largest second harmonics the temperature gradient are higher at these frequencies.

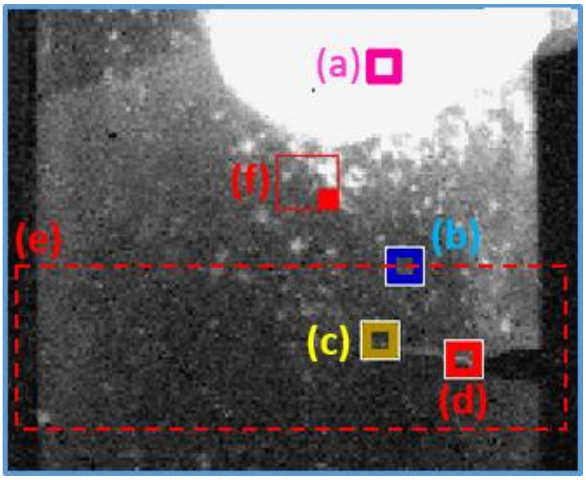

Figure 12: Location of temperature profiles for sensor (a), surface point (b), crack tip (c), crack point (d), crack focus window (e) and IR focus area (f).

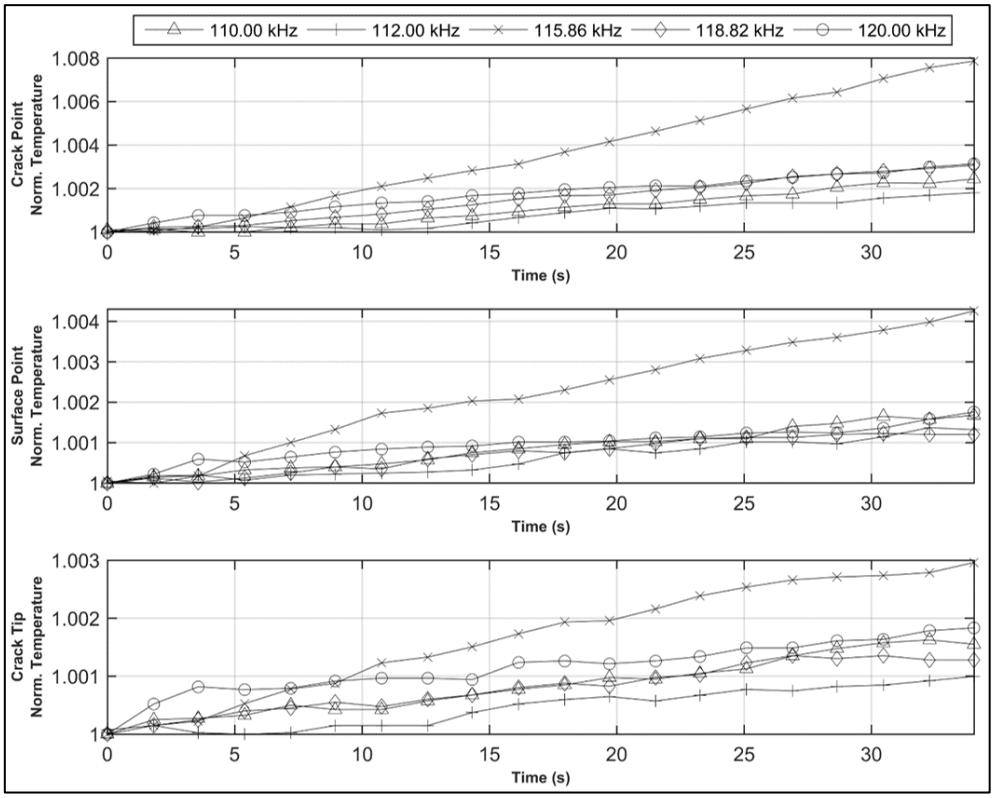

Figure 13: Best fundamental (f_1) and random frequencies relative temperature profiles for positions at the crack point, surface point and crack tip.

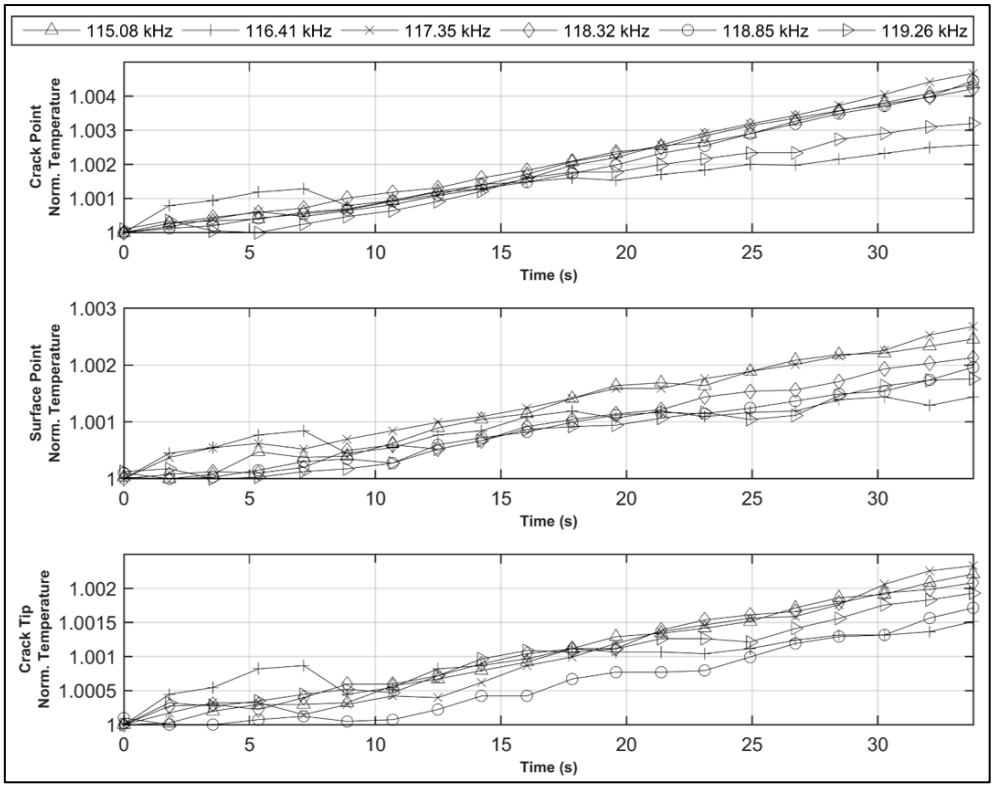

Figure 14: Best second harmonic ($2f_1$) relative temperature profiles for positions at the crack point, surface point and crack tip.

Figure 15 shows the temperature distribution images captured during NUST for the various defect resonance frequencies tested.

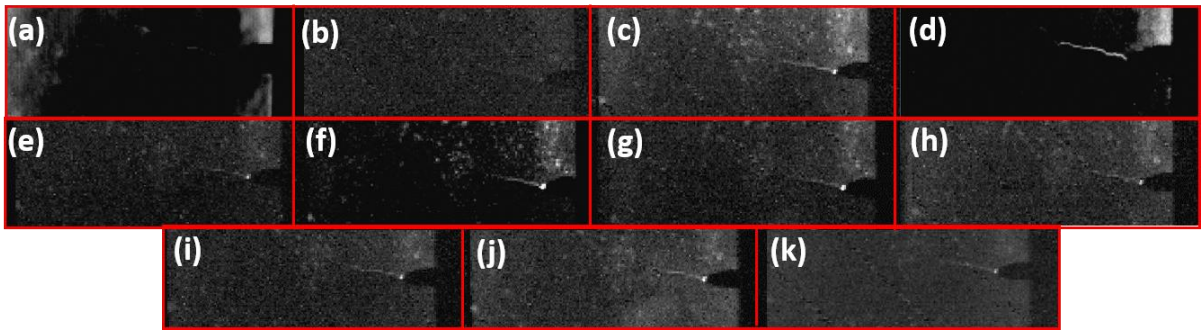

Figure 15: IR camera results for crack heating at specific defect resonance excitation frequencies: 110 kHz (a), 112 kHz (b), 115.078 kHz (c), 115.859 kHz (d), 116.406 kHz (e), 117.345 kHz (f), 118.32 kHz (g), 118.75 kHz (h), 118.82 kHz (i), 119.26 kHz (j) and 120 kHz (k).

The normalised thermal gradients for each defect resonance frequency and position are highlighted in Figure 16 below. The highest thermal gradients refer to the frequencies that provided the greatest average second harmonic responses over the inspected region with the exception of 115859 Hz. Although as it will be shown later, local frequency response around the cracked region shows that the largest second harmonic in terms of frictional heating is in fact at 115859 Hz. This demonstrates that the combination and interaction between f_1 and the nonlinear vibration modes ($2f_1$) near the crack interface can have a large effect on the generation of heat, and ultimately the effectiveness of the method.

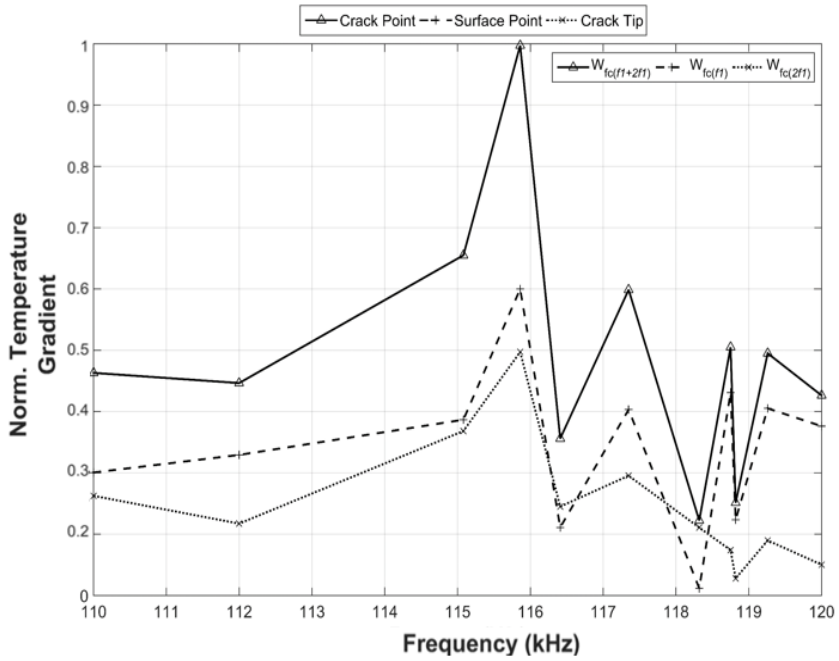

Figure 16: Relative thermal gradients for various frequencies tested for positions at the crack point, surface point, sensor point and end of the crack**.**

In order to assess the effect of nonlinearity around the cracked region, β_{ratio} [Figure 17(e), sparse dotted line] was calculated by determining the average of the ratio of the $\beta_{damaged}$ [(Figure 17(b) and (d)] over the $\beta_{undamaged}$ [Figure 17(a) and (c)], according to Eq. (6). In practise, the ratio of the second harmonic and fundamental squared amplitudes obtained from FFT responses at each grid location of the damaged and undamaged area was calculated and averaged in order to get the β_{ratio}. This process was then repeated for each excitation frequency.

By then comparing the β_{ratio} to the relative temperature profile (normalised) it is clear that the production of nonlinearities are in line with the heat generated at the cracked region.

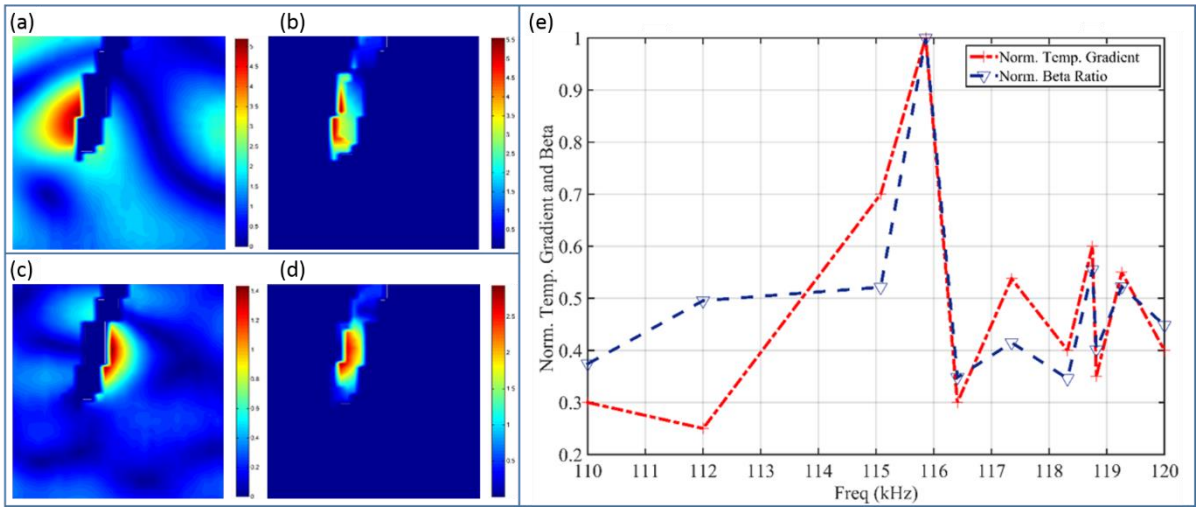

Figure 17 The fundamental frequency response (a-b) and second harmonic response (c-d) for the damaged (b-d) and undamaged (a-c) regions relating to 115859 Hz used for nonlinear assessment of β_{ratio}, and the relative temperature gradient at the crack point vs. normalised beta ratio over the range of frequencies tested (e).

Moreover, the heat generated by the individual frequency components was assessed by calculating the frictional work contribution for both the defect resonance and second harmonic responses (Figure 18

(a) and (b)). According to Eq. (4), W_{fc} was calculated by determining the change in velocity for LV scanned points that outlined the crack for both f_1 and $2f_1$, with T (time of excitation) being considered constant. As can be seen by Figure 18 (a) and (b), the local frequency response near the crack differs from those outlined in Figure 4 (a) and (b), which highlights the difficulty in determining the defect resonance frequency. By adding the frictional work contribution generated by $2f_1$ to f_1 the effect of this nonlinearity on heating can be assessed.

The profile of combined friction work contribution versus the fundamental (f_1) contribution is very similar, although according to Figure 18 (a) the frictional work contribution (and therefore heat) produced at 115080 Hz (C) should be less than at 117350 Hz (F), 118750 Hz (H) and 119260 Hz (J). However, after taking into account heating due to the second harmonic, the contribution is greater at C than F, H and J. These results are confirmed in Figure 17(e) where the relative temperature gradient recorded using the IR camera shows that heating is in fact larger at C. The fact that heating generated at H and J (Figure 17(e)) is greater than F, suggests that the out-of-plane velocity at these frequencies are insufficient to explain the full extent of the heating mechanism (as further heating is due to in-plane clapping or rubbing, and normal forces acting on the interface).

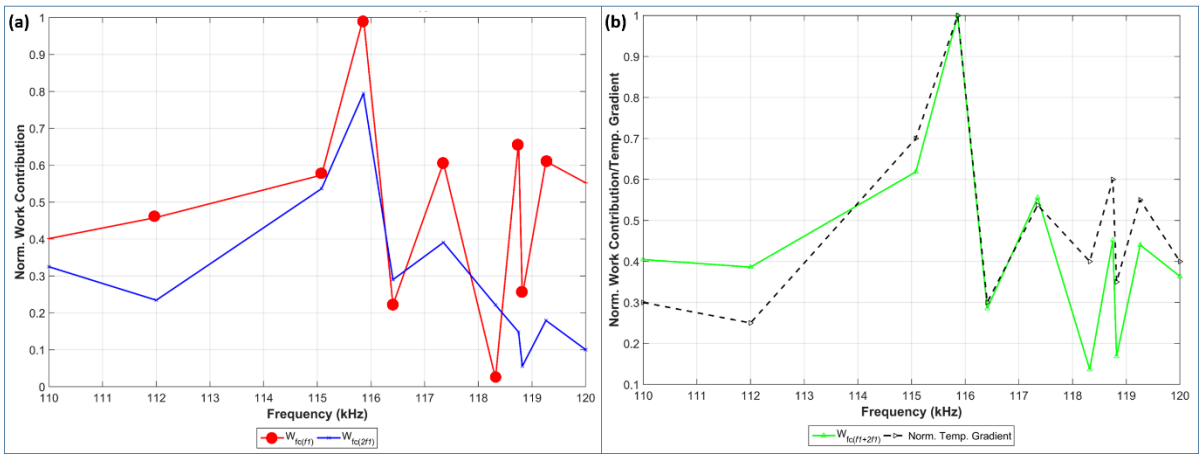

Figure 18: Frictional work contribution calculated from out-of-plane velocity (near crack) according to the: (a) fundamental frequency (f_1) response (solid and dotted line) and second harmonic response ($2f_1$) (solid line) and (b) the total of the fundamental and second harmonic responses (f_1 + $2f_1$) (solid line) vs. relative temperature gradient (dotted line).

1.7. Conclusions

A novel Nonlinear Ultrasound Stimulated Thermography technique is proposed to overcome the limitations of traditional linear ultrasound/thermography NDE-SHM systems and to provide a reliable, rapid and cost effective estimation of fatigue damage in isotropic materials. This novel methodology relies on the evaluation of a novel nonlinear ultrasound parameter (β_{ratio}) which was used to compare the material nonlinear responses at the damaged and undamaged regions. The β_{ratio} was then compared to the relative temperature gradients for various frequencies at the damage location and showed good correlation. Thus, by understanding the frequencies that give rise to high nonlinear harmonic response in the damaged material and exciting at the corresponding fundamental frequencies, an increase in the probability of damage detection was observed. This work also found that the additional interactions between the second harmonic ($2f_1$) and the damage interface cannot be discounted when trying to generate optimal heating conditions for damage/defect evaluation, therefore the combination and interaction of linear and nonlinear effects within the heating process have a great influence on heat production. This was confirmed by assessing the frictional work contribution related to the fundamental (f_1) and second harmonic ($2f_1$) and comparing them to the relative temperature gradients for various frequencies tested, which showed good similarities. FEA was used to assess the modal shapes for the damaged and undamaged structure; these results show the importance of the location of local minima

and maxima displacements with respect to the damaged region. The FEA results highlighted the potential of using modal analysis to estimate which frequencies are likely to give rise to large interface interactions (friction) in a region where fatigue damage is likely to occur. Finally, experimental and numerical results showed that heat generation at damaged regions could be amplified by exciting at frequencies that provide high nonlinear responses, leading to improved and quicker imaging of material damage and enhancing the reliability of the proposed Nonlinear Ultrasound Stimulated Thermography approach.

Acknowledgment

This work was funded by project ALAMSA of the European Union's Seventh Framework Programme for research, technological development and demonstration under grant agreement number 314768.

1.8. References

[1]. Bartelds G. Aircraft structural health monitoring, prospects for smart solutions from a European viewpoint Structural Health Monitoring. Current Status and Perspectives, Proc. Int. Workshop on Structural Health Monitoring (Stanford, CA, Sept. 1997) ed. F-K Chang (Lancaster, PA: Technomic), 293-300, 1997.

[2]. Blitz, J., & Simpson, G. Ultrasonic methods of non-destructive testing. Vol. 2. Springer Science & Business Media, 1995.

[3]. Almond, D.P, and Pickering, S.G, "An analytical study of the pulsed thermography defect detection limit". J. Appl. Phys. 111:093510, 2012.

[4]. Morbidini, M, Cawley, P. "A calibration procedure for sonic infrared non-destructive evaluation". J. Appl. Phys. 106:023504, 2009.

[5]. Meyendorf, N. G., Rösner, H., Kramb, V. and Sathish, S., (2002), Thermo-acoustic fatigue characterization, Ultrasonics 40, pp. 427-434.

[6]. Han, X., Favro, L. and Thomas, R., (2003), Review of Progress in Quantitative Nondestructive Evaluation 22, ed, By DO Thompson and DE Chimenti, Am. Inst. Phys. CP657, pp. 500-504.

[7]. Ciampa, F., Scarselli, G., Pickering, S., Meo, M. Nonlinear elastic wave tomography for the imaging of corrosion damage. Ultrasonics, 62, pp. 147-155, 2015.

[8]. Ciampa, F., Meo, M. "Nonlinear elastic imaging using reciprocal time reversal and phase symmetry analysis". Journal of Acoustical Society of America, 130 (6), pp. 4316-4323, 2012.

[9]. Zumpano, G., Meo, M. "Damage localization using transient non-linear elastic wave spectroscopy on composite structures," International Journal of Non-Linear Mechanics, 43: 217 – 230, 2008.

[10]. Donskoy, D., Sutin, A., & Ekimov, A., Donskoy, D., A. Sutin, and A. Ekimov. "Nonlinear acoustic interaction on contact interfaces and its use for nondestructive testing." Ndt & E International, 34(4), 231-238, 2001.

[11]. Nagy PB, Adler L. Acoustic nonlinearities in plastics. In: Thompson DO, Chimenti DE, editors. Review of progress in quantitative non-destructive evaluation, vol. 11, 1992.

[12]. Ciampa, F., Meo, M. Nonlinear elastic imaging using reciprocal time reversal and phase symmetry analysis. Journal of Acoustical Society of America, 130 (6), pp. 4316-4323, 2012.

[13]. Landau, L. D., & Lifshitz, E. M. "Theory of Elasticity, vol. 7." Course of Theoretical Physics 3, 109, 1986.

[14]. De Angelis, G., Meo, M., Almond, D.-P., Pickering, S. G., Angioni, S.-L. "A new technique to detect defect size and depth in composite structures using digital shearography and unconstrained optimization". NDT E Int. 45, pp. 91–96, 2012.

[15]. Solodov, I., Bai, J., Bekgulyan, S., & Busse, G. A local defect resonance to enhance acoustic wave-defect interaction in ultrasonic nondestructive evaluation. Applied Physics Letters, 99(21), 211911, 2011.

[16]. Reifsnider, K., Henneke, E. G. and Stinchcomb, W., (1980), The mechanics of vibrothermography, Mechanics of nondestructive testing, pp. 249-276.

[17]. Pippard, A., (1978), The physics of vibration. Vol. 1: The simple classical vibrator, Cambridge: University Press, 1978 1.
[18]. Homma, C., Rothenfusser, M., Baumann, J. and Shannon, R., Quantitative Nondestructive Evaluation, AIP Publishing, 2006, pp. 566-573.
[19]. Cantrell, J. H. and Yost, W. T., (2001), Nonlinear ultrasonic characterization of fatigue microstructures, International Journal of fatigue 23, pp. 487-490.
[20]. Fierro, G. M., Ciampa, F., Ginzburg, D., Onder, E. and Meo, M., (2015), Nonlinear ultrasound modelling and validation of fatigue damage, Journal of Sound and Vibration 343, pp. 121-130.
[21]. Cantrell, J. H., (2004), Fundamentals and applications of non-linear ultrasonic nondestructive evaluation, Ultrasonic non-destructive evaluation vol. 6, pp. p.363-434.